

Soft and transferable pseudopotentials from multi-objective optimization

Mostafa Faghih Shojaei^a, John E. Pask^b, Andrew J. Medford^a, Phanish Suryanarayana^{a,*}

^aCollege of Engineering, Georgia Institute of Technology, Atlanta, GA 30332, USA

^bPhysics Division, Lawrence Livermore National Laboratory, Livermore, CA 94550, USA

Abstract

Ab initio pseudopotentials are a linchpin of modern molecular and condensed matter electronic structure calculations. In this work, we employ multi-objective optimization to maximize pseudopotential softness while maintaining high accuracy and transferability. To accomplish this, we develop a formulation in which softness and accuracy are simultaneously maximized, with accuracy determined by the ability to reproduce all-electron energy differences between Bravais lattice structures, whereupon the resulting Pareto frontier is scanned for the softest pseudopotential that provides the desired accuracy in established transferability tests. We employ an evolutionary algorithm to solve the multi-objective optimization problem and apply it to generate a comprehensive table of optimized norm-conserving Vanderbilt (ONCV) pseudopotentials (<https://github.com/SPARC-X/SPMS-psps>). We show that the resulting table is softer than existing tables of comparable accuracy, while more accurate than tables of comparable softness. The potentials thus afford the possibility to speed up calculations in a broad range of applications areas while maintaining high accuracy.

Keywords: Pseudopotential, Norm conservation, PBE, Density functional theory, Electronic structure, Evolutionary algorithm

1. Introduction

Over the past few decades, Kohn–Sham density functional theory (DFT) [1, 2] has established itself as a cornerstone of physical, chemical, and materials research, enabling the study of a wide variety of systems from the first principles of quantum mechanics, with no empirical or adjustable parameters. The popularity of DFT can be attributed to its high accuracy-to-cost ratio relative to other such ab initio methods, particularly in the context of the widely adopted pseudopotential approximation [3]. In this approach, core electrons not participating in the chemistry of interest are removed from the calculation by replacing the Coulomb potential of the nucleus by an effective potential corresponding to the nucleus and frozen core electrons, referred to as a pseudopotential. The goal of such a strategy is to significantly reduce the computational cost of the calculations while keeping the physical/chemical properties of the system sufficiently unchanged.

The pseudopotential formulations most widely employed in modern Kohn-Sham calculations are of three main kinds: ultrasoft [4]; projector-augmented-wave (PAW) [5]; and norm-conserving, such as Hamann-Schlüter-Chiang (HSC) [6], Kerker [7], Bachelet-Hamann-Schlüter (BHS) [8], generalized norm-conserving [9], Rappe-Rabe-Kaxiras-Joannopoulos (RRKJ) [10], Troullier-Martins (TM) [11], Goedecker-Teter-Hutter

*Corresponding Author (phanish.suryanarayana@ce.gatech.edu)

(GTH) [12], Hartwigsen-Goedecker-Hutter (HGH) [13], and Hamann’s optimized norm-conserving Vanderbilt (ONCV) [14] potentials. Among these, ultrasoft and PAW are typically softer than norm-conserving potentials, i.e., a larger grid spacing in real-space calculations or smaller energy cutoff in plane-wave calculations suffices to achieve a specified accuracy with respect to discretization. However, ultrasoft and PAW formulations lead to a generalized rather than standard eigenvalue problem, even within orthonormal discretization schemes. This can increase computational cost and limit parallel scalability, in real-space methods [15, 16, 17] in particular, where efficient and scalable preconditioners for the eigenvalue problem are lacking. In addition, the PAW formulation introduces complexities in deriving and implementing expressions involving derivatives, such as atomic forces, stress tensor, and phonons. These and other issues have motivated the further development of norm-conserving pseudopotentials in recent works [14, 18, 19].

The generation of soft and transferable norm-conserving pseudopotentials can, however, be a challenging task. To simplify the process of performing DFT simulations, a number of pseudopotential tables, i.e., sets of pseudopotentials covering most of the periodic table, have been generated. These include (i) ultrasoft: Garrity-Bennett-Rabe-Vanderbilt (GBRV) [20]; (ii) PAW: VASP [21], Jollet-Torrent-Holzwarth (JTH) [22], Topsakal-Wentzcovitch [23]; (iii) norm-conserving: BHS [8], GTH [12], HGH [24], PARSEC [25], Fritz-Haber-Institute (FHI) [26], Krack [24], Willand et al. [27], Schlipf-Gygi (SG15) [18], and PseudoDojo [19]; and (iv) mixtures of these types: pslibrary [28, 29] and SSSP [30]. However, though these pseudopotentials have been tested for their accuracy, apart from SG15 [18], where a metric including both accuracy (in terms of lattice constant error) and softness was maximized, the pseudopotentials have not been generated through a systematic optimization process. This makes the generation of pseudopotential tables an arduous and time consuming task, particularly given the large number of variants of interest in practice: exchange-correlation functionals, relativistic effects, core-valence partitions, and the like. In addition, it is likely that these pseudopotentials are harder than necessary for the accuracy they provide.

In this work, we employ multi-objective optimization to maximize pseudopotential softness while maintaining high accuracy and transferability. To accomplish this, we develop a formulation in which softness and accuracy are simultaneously maximized, with accuracy determined by the ability to reproduce all-electron energy differences between Bravais lattice structures, whereupon the resulting Pareto frontier is scanned for the softest pseudopotential that provides the desired accuracy in established transferability tests. We employ the optimization scheme to generate a table of ONCV pseudopotentials for sixty-nine chemical elements (H–La and Hf–Bi) within the Perdew–Burke–Ernzerhof (PBE) [31] exchange-correlation approximation (<https://github.com/SPARC-X/SPMS-psps>). We show that the resulting table is softer than recent tables of comparable accuracy, while more accurate than recent tables of comparable softness.

The remainder of this paper is organized as follows. In Section 2, we develop a formulation for generating soft and transferable pseudopotentials. In Section 3, we provide an overview of the ONCV pseudopotential formalism. In Section 4, we describe the implementation for generating soft and transferable ONCV pseudopotentials. In Section 5, we discuss some representative results as well as the accuracy and softness of the table of ONCV pseudopotentials generated. Finally, we provide concluding remarks in Section 6.

2. Formulation

We now present an approach for generating soft and transferable pseudopotentials within any given pseudopotential formalism. In particular, we consider the following multi-objective optimization problem:

$$\mathbf{p}^* = \arg \min_{\mathbf{p} \in P} \left(\mathcal{E}(\mathbf{p}), \frac{1}{\mathcal{S}(\mathbf{p})} \right), \quad (1)$$

where \mathbf{p} is the vector of parameters that characterize the pseudopotential, P is the feasible set of all such vectors, and \mathcal{E} and \mathcal{S} are metrics that measure the error and softness of the pseudopotential, respectively. Note that these metrics measure distances with respect to the all-electron Coloumb potential, and have been written as a function of \mathbf{p} to indicate the dependence of the calculated values on \mathbf{p} . Since \mathcal{E} and $1/\mathcal{S}$ have an overall negative correlation with each other, the solution of the above minimization problem is a Pareto set/frontier, i.e., for any pseudopotential that does not belong to the Pareto frontier, there exists at least one pseudopotential in the Pareto frontier that has smaller values for both \mathcal{E} and $1/\mathcal{S}$.

A natural variable for defining the softness metric \mathcal{S} is the grid spacing used in real-space calculations, or equivalently, the inverse of the energy cutoff used in planewave calculations. However, there is no such computationally tractable *universal* error metric \mathcal{E} , i.e., one that captures the accuracy of the pseudopotential for every possible electronic environment encountered in molecular and condensed matter systems. Indeed, if such a *universal* \mathcal{E} were to be available, then the softest pseudopotential for the desired accuracy can immediately be chosen from the generated Pareto frontier. In view of this, we reformulate the optimization problem in Eq. 1 as the following two-step scheme:

$$\hat{\mathbf{p}} = \arg \min_{\mathbf{p} \in P} \left(\mathcal{E}_0(\mathbf{p}), \frac{1}{\mathcal{S}(\mathbf{p})} \right), \quad (2a)$$

$$\mathbf{p}^* = \arg \min_{\mathbf{p} \in P_f} \frac{1}{\mathcal{S}(\mathbf{p})}, \quad P_f = \{\hat{\mathbf{p}} : \mathcal{E}_i(\hat{\mathbf{p}}) \leq \epsilon_i, i = 1, 2, \dots, n\}, \quad (2b)$$

where \mathcal{E}_0 is some relatively simple and computationally efficient error metric that is used in the multi-objective optimization, and $\{\mathcal{E}_i\}_{i=1}^n$ are the more sophisticated and likely more computationally expensive error metrics to be used in choosing the pseudopotential from the Pareto frontier, with $\{\epsilon_i\}_{i=1}^n$ being the desired upper bounds on these errors. Within this reformulation, the error metric \mathcal{E}_0 is expected to reliably estimate the accuracy and transferability of the pseudopotential, while simultaneously ensuring that the computational cost associated with the optimization is tractable. A maximally soft pseudopotential from the Pareto frontier with the desired accuracy and transferability for the physical/chemical application of interest can then be selected by suitably choosing $\{\mathcal{E}_i\}_{i=1}^n$ and $\{\epsilon_i\}_{i=1}^n$.

We propose the use of a structural energy difference based error metric in the multi-objective optimization (Eq. 2a):

$$\mathcal{E}_0 := \delta_{\Delta E} = \frac{1}{\sqrt{14m}} \|\Delta \mathbf{E}^{\text{psp}} - \Delta \mathbf{E}^{\text{ae}}\|_2, \quad (3a)$$

$$\Delta \mathbf{E}^{\text{psp/ae}} = (E_1^{\text{psp/ae}} - E_0^{\text{psp/ae}}, E_2^{\text{psp/ae}} - E_0^{\text{psp/ae}}, \dots, E_{14m}^{\text{psp/ae}} - E_0^{\text{psp/ae}}), \quad (3b)$$

where $\{E_i^{\text{psp}}\}_{i=1}^{14m}$ and $\{E_i^{\text{ae}}\}_{i=1}^{14m}$ are the Kohn-Sham energies for a set of $14m$ primitive Bravais lattices containing structures with the 14 Bravais lattice symmetries (Fig. 1) with m different nearest neighbor distances. In addition, $E_0^{\text{psp/ae}}$ is a reference energy to ensure meaningful comparison between pseudopotential and all-electron results. Such a choice for \mathcal{E}_0 can be interpreted as follows: the primitive Bravais lattices represent a basis for sampling the various electronic environments that are encountered within materials systems. Indeed, the basis can be made more complete by considering Bravais lattices with a basis that have two or more different chemical elements. However, this comes with significant additional computational cost and complexity, and hence not considered in this work. For the softness metric, we choose the following:

$$\mathcal{S} = \frac{1}{E_{\text{cut}}}, \quad (4)$$

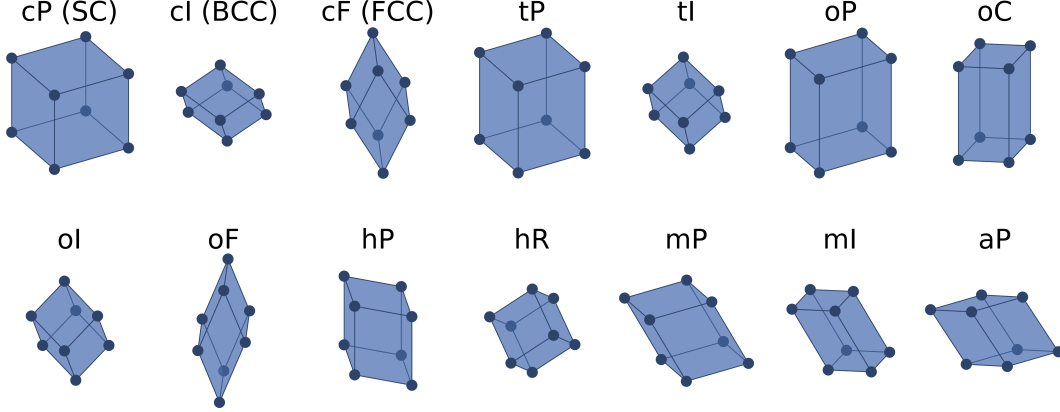


Figure 1: The set of 14 Bravais lattice symmetries used for defining the error metric $\delta_{\Delta E}$ in the multi-objective optimization (Eq. 5a).

where E_{cut} is the planewave energy cutoff required to achieve a desired accuracy with respect to discretization in pseudopotential calculations. Note that in defining the softness metric, we have set the softness of the all-electron Coloumb potential to be zero. Once the optimization problem has been solved for the Pareto frontier, we choose the following error metrics for selecting the pseudopotential (Eq. 2b): Δ -factor [32], lattice constant error δ_{lat} , error associated with the acoustic sum rule in phonon calculations δ_{asr} , and error in phonon frequencies δ_{ω} corresponding to a specified error in energy, having imposed the acoustic sum rule. Indeed, these error metrics have been commonly used in literature to check the accuracy of pseudopotentials [33, 19, 30]. Thereafter, the optimization problem for generating soft and transferable pseudopotentials can be written as:

$$\hat{\mathbf{p}} = \arg \min_{\mathbf{p} \in P} (\delta_{\Delta E}(\mathbf{p}), E_{\text{cut}}(\mathbf{p})), \quad (5a)$$

$$\mathbf{p}^* = \arg \min_{\mathbf{p} \in P_f} E_{\text{cut}}(\mathbf{p}), \quad P_f = \{\hat{\mathbf{p}} : \Delta(\hat{\mathbf{p}}) \leq \epsilon_1, \delta_{\text{lat}}(\hat{\mathbf{p}}) \leq \epsilon_2, \delta_{\text{asr}}(\hat{\mathbf{p}}) \leq \epsilon_3, \delta_{\omega}(\hat{\mathbf{p}}) \leq \epsilon_4\}, \quad (5b)$$

where the parameters that are being optimized \mathbf{p} and the feasible set P are dependent on the type of pseudopotential under consideration.

3. ONCV pseudopotential formalism

We now briefly review the ONCV pseudopotential formalism for completeness, the details of which can be found in Refs. [14, 34]. The atomic nonlocal ONCV pseudopotential operator can be written as

$$V_{\text{nl}}^{\ell} = \sum_{i,j=1}^{P^{\ell}} |\chi_i^{\ell}\rangle (B^{\ell})^{-1}_{ij} \langle \chi_j^{\ell}| = \sum_{i=1}^{P^{\ell}} |\tilde{\chi}_i^{\ell}\rangle \frac{1}{\tilde{b}_i^{\ell}} \langle \tilde{\chi}_i^{\ell}|, \quad B_{ij}^{\ell} = \langle \varphi_i^{\ell} | \chi_j^{\ell} \rangle, i, j = 1, \dots, P^{\ell}, \quad \ell = 0, \dots, L, \quad (6)$$

where φ_i^{ℓ} are the radial pseudo-wavefunctions, L is the maximum angular momentum, and

$$|\chi_i^{\ell}\rangle = (\varepsilon_i^{\ell} - T^{\ell} - V_{\text{loc}}) |\varphi_i^{\ell}\rangle, \quad i = 1, \dots, P^{\ell}, \quad (7)$$

are the projectors obtained by φ_i^{ℓ} at energy ε_i^{ℓ} . In addition, \tilde{b}_i^{ℓ} are the eigenvalues of B^{ℓ} and $\tilde{\chi}_i^{\ell}$ are linear combinations of χ_i^{ℓ} with coefficients derived from the eigenvectors, after having normalized χ_i^{ℓ} and appropriately rescaled B^{ℓ} . In Eq. 7, $T^{\ell} = [-d^2/dr^2 + \ell(\ell+1)/r^2]/2$ is the kinetic energy operator, and V_{loc} is

the local potential operator that smoothly joins to the all-electron potential V_{ae} at radius r_{loc} , being arbitrary otherwise. Let ψ_i^ℓ be the all-electron wave function corresponding to φ_i^ℓ . Note that $\varphi_i^\ell(r) = \psi_i^\ell(r)$ for $r > r_c^\ell$, $\ell = 0, \dots, L$ and $r_{\text{loc}} \leq \min_{\ell=0, \dots, L} r_c^\ell$, where r_c^ℓ is the cutoff radius for angular momentum channel ℓ . The pseudo-wavefunctions are required to satisfy M^ℓ continuity constraints at r_c^ℓ :

$$\left. \frac{d^m \varphi_i^\ell}{dr^m} \right|_{r_c^\ell} = \left. \frac{d^m \psi_i^\ell}{dr^m} \right|_{r_c^\ell}, \quad m = 0, \dots, M^\ell - 1, \quad i = 1, \dots, P^\ell, \quad \ell = 0, \dots, L, \quad (8)$$

as well as the generalized norm-conservation constraint:

$$\langle \varphi_i^\ell | \varphi_j^\ell \rangle_{r_c^\ell} = \langle \psi_i^\ell | \psi_j^\ell \rangle_{r_c^\ell}, \quad i, j = 1, \dots, P^\ell, \quad \ell = 1, \dots, L, \quad (9)$$

where the subscripts r_c^ℓ indicates that the domain of calculation is $[0, r_c^\ell]$. Note that B^ℓ and therefore V_{nl}^ℓ are Hermitian if the norm-conservation constraint (Eq. 9) is satisfied [4].

The pseudo-wavefunctions arising in the above expressions are determined as follows. For a given ℓ , one can write the spherical Fourier transform of $\varphi_i^\ell(r)$ as $\bar{\varphi}_i^\ell(q) = \int_0^\infty j_\ell(qr) \varphi_i^\ell(r) r^2 dr$, where j_ℓ is a spherical Bessel function. Then, by considering a cutoff wavevector q_c^ℓ , one can define the following residual kinetic energies:

$$E_{ij}^\ell(q_c^\ell) = \int_{q_c^\ell}^\infty \bar{\varphi}_i^\ell(q) \bar{\varphi}_j^\ell(q) q^4 dq \equiv \langle \bar{\varphi}_i^\ell | \hat{E}^\ell(q_c^\ell) | \bar{\varphi}_j^\ell \rangle, \quad i, j = 1, \dots, P^\ell, \quad \ell = 0, \dots, L. \quad (10)$$

Thereafter, the optimization problem for the pseudo-wavefunctions can be stated as follows: given ℓ , q_c^ℓ , r_c^ℓ , M^ℓ , and P^ℓ , find a set of pseudo-wavefunctions φ_i^ℓ , $i = 1, \dots, P^\ell$, that minimizes the resulting kinetic energies (Eq. 10) subject to continuity constraints (Eq. 8) and norm-conservation constraint (Eq. 9). To satisfy the continuity constraints (Eq. 8), one first constructs a set of N^ℓ orthonormalized spherical Bessel functions $\xi_n^{\text{O}\ell}$ such that $\xi_n^{\text{O}\ell} = 0$ for $r > r_c^\ell$, and writes $\varphi^\ell = \sum_{n=1}^{N^\ell} z_n^\ell \xi_n^{\text{O}\ell}$. For simplicity, the subscript i of φ_i^ℓ is ignored as this applies to all pseudo-wavefunctions with $i = 1, \dots, P^\ell$. One then substitutes φ^ℓ into Eq. 8 and uses singular value decomposition to solve the resulting system of M^ℓ linear equations in terms of N^ℓ unknowns z_i^ℓ , $i = 1, \dots, N^\ell$. The solution gives $\varphi_0^\ell = \sum_{n=1}^{N^\ell} z_{0n}^\ell \xi_n^{\text{O}\ell}$, $r \leq r_c^\ell$; $\varphi_0^\ell = \psi^\ell$, $r > r_c^\ell$ and the basis functions $\xi_n^{\text{N}\ell}$, $n = 1, \dots, N^\ell - M^\ell$, spanning the null space of the linear system provided that $N^\ell > M^\ell$. Note that $\xi_n^{\text{N}\ell}$, $n = 1, \dots, N^\ell - M^\ell$, are orthonormal, orthogonal to φ_0^ℓ , and have $M^\ell - 1$ derivatives at r_c^ℓ . To further simplify the optimization problem, one can calculate the eigenvalues e_n^ℓ and eigenvectors of the matrix generated by $\langle \xi_n^{\text{N}\ell} | \hat{E}^\ell | \xi_s^{\text{N}\ell} \rangle$, and then define a set of ‘‘residual’’ basis functions $\xi_n^{\text{R}\ell}$ as linear combinations of $\xi_n^{\text{N}\ell}$ with coefficients derived from the eigenvectors such that $\langle \xi_n^{\text{R}\ell} | \hat{E}^\ell | \xi_s^{\text{R}\ell} \rangle = e_n^\ell \delta_{ns}$, $n, s = 1, \dots, N^\ell - M^\ell$. Now, by satisfying Eq. 8 and modifying Eq. 9 and Eq. 10 with the general solution:

$$\varphi^\ell = \varphi_0^\ell + \sum_{n=1}^{N^\ell - M^\ell} x_n^\ell \xi_n^{\text{R}\ell}, \quad (11)$$

the optimization problem for finding a pseudo-wavefunction φ^ℓ can be simplified to read: given ℓ , q_c^ℓ , r_c^ℓ , M^ℓ , and $N^\ell > M^\ell$, find x_n^ℓ , $n = 1, \dots, N^\ell - M^\ell$, such that

$$E^\ell = E_{00}^\ell + \sum_{n=1}^{N^\ell - M^\ell} (2f_n^\ell x_n^\ell + e_n^\ell (x_n^\ell)^2), \quad (12)$$

where $E_{00}^\ell = \langle \varphi_0^\ell | \hat{E}^\ell | \varphi_0^\ell \rangle$, and the ‘‘force’’ terms $f_n^\ell = \langle \varphi_0^\ell | \hat{E}^\ell | \zeta_n^{\text{R}\ell} \rangle$ are minimized subject to norm-conservation constraint:

$$\sum_{n=1}^{N^\ell - M^\ell} (x_n^\ell)^2 = \langle \psi^\ell | \psi^\ell \rangle_{r_c} - \sum_{n=1}^{N^\ell} (z_{0n}^\ell)^2 \equiv D_{\text{norm}}^\ell. \quad (13)$$

Above, D_{norm}^ℓ is the ‘‘norm deficit’’ of φ_0^ℓ relative to norm of ψ^ℓ on $[0, r_c^\ell]$.

4. Implementation

We have implemented the formulation described in Section 2 for the automated generation of soft and transferable ONCV pseudopotentials. In particular, we have developed a framework in `python` that uses ONCVSP [35] for generation of the pseudopotentials, ABINIT [36] for pseudopotential DFT calculations, and Elk [37] for reference all-electron (i.e., Coulomb potential) DFT calculations. Given the large computational cost associated with Kohn-Sham DFT calculations, the framework is capable of running ABINIT as well as Elk in parallel, allowing for significant reduction in the time to solution of the optimization problem described by Eqs. 5a and 5b.

We choose the following ONCV pseudopotential parameters (Section 3):

$$\mathbf{p} = (\{r_c^\ell\}_{\ell=0}^L, \{q_c^\ell\}_{\ell=0}^L, \{N^\ell\}_{\ell=0}^L, \{M^\ell\}_{\ell=0}^L, r_{\text{loc}}), \quad (14)$$

where $\{r_c^\ell\}_{\ell=0}^L$ are the cutoff radii for the nonlocal projectors, $\{q_c^\ell\}_{\ell=0}^L$ are the cutoff wavevectors for the pseudo-wavefunctions’ residual kinetic energies, $\{N^\ell\}_{\ell=0}^L$ are the number of basis functions used for the pseudo-wavefunctions, $\{M^\ell\}_{\ell=0}^L$ are the number of continuity constraints at $\{r_c^\ell\}_{\ell=0}^L$, and r_{loc} is the cutoff radius for the local part of the pseudopotential. The remaining parameters in the ONCV formalism are held fixed at prespecified values, which in the current work are the same as in the PseudoDojo standard-accuracy PBE table [19]. For the feasible set, we choose:

$$P = \left\{ \mathbf{p} : \{r_c^\ell\}_{\ell=0}^L \in [1, r_u], \{q_c^\ell\}_{\ell=0}^L \in [1, 14], \{N^\ell\}_{\ell=0}^L \in \{7, 8, 9\}, \right. \\ \left. \{M^\ell\}_{\ell=0}^L = 4, r_{\text{loc}} \in [0.2, \min\{r_c^\ell\}_{\ell=0}^L] \right\}, \quad (15)$$

which is generally decided on empirical considerations.

In the multi-objective optimization (Eq. 5a), we choose $\delta_{\Delta E}$ to be the error metric corresponding to structural energy differences for the 14 Bravais lattice symmetries (i.e., $m = 1$), each with the nearest neighbor distance set to the equilibrium lattice constant for a simple cubic crystal, as determined from all-electron calculations using Elk. In isolated cases where the simple cubic crystal did not yield representative distances, the nearest neighbor distance was set instead based on known equilibrium distances. To reduce the computational cost of the optimization, we use a surrogate for E_{cut} , namely \tilde{E}_{cut} , which is defined to be the maximum cutoff energy over the different angular momentum channels (i.e., ℓ) for kinetic energy convergence error of 10^{-5} Ha. This number is immediately available from the ONCVSP code upon generation of the pseudopotential, and has been found to correlate well with the planewave energy cutoff E_{cut} . Also, in order to eliminate pseudopotentials that have large errors in logarithmic derivatives and/or result in ghost states at lower energies, we augment the optimization problem with penalty functions within the implementation.

We solve the multi-objective optimization (Eq. 5a) using the improved strength Pareto evolutionary algorithm (SPEA2) [38]. The motivation for choosing an evolutionary algorithm is that (i) it does not require the calculation of derivatives of $\delta_{\Delta E}$ and E_{cut} with respect to \mathbf{p} , quantities that are not readily available in the current context, and (ii) the optimization problem is a mixed-integer non-linear problem with a computationally expensive black-box objective function. During the optimization process, we choose the following settings in ABINIT and Elk: Fermi-Dirac smearing of 0.001 Ha, and $4 \times 4 \times 4$ Monkhorst-Pack grid for Brillouin zone integration with (0.5, 0.5, 0.5) shift. In addition, we use planewave cutoff $E_{\text{cut}} = 60$ Ha in ABINIT and the highest accuracy `vhighq` option in Elk. Note that the all-electron Elk simulations need to be performed only once at the beginning of the optimization. In fact, storing the results allows for reuse in any subsequent efforts to generate pseudopotentials within the proposed formulation.

Once the Pareto frontier has been determined, we evaluate the values of the error metrics Δ , δ_{lat} , δ_{asr} , and δ_{ω} for all the pseudopotentials belonging to this set. In particular, we calculate the Δ -factor using the formalism/codes presented in Ref. [32] (with input files for ABINIT taken from Ref. [19]) which is set to Δ (meV/atom); percentage error in lattice constants for structures used to test the GBRV pseudopotentials [20], the mean of which is set to δ_{lat} (%); acoustic sum rule error corresponding to the highest and lowest acoustic frequencies (HAP and LAP, respectively) at the Γ -point for the Δ -factor lattice structures, the mean of which is set to δ_{asr} (cm^{-1}); and percentage phonon frequency error for the highest and lowest phonon frequencies (HOP and LOP, respectively, obtained after imposing the acoustic sum rule) at the Γ -point for the Δ -factor lattice structures, corresponding to an accuracy of 10^{-4} Ha/atom in the energy, the mean of which is set to δ_{ω} (%). For the ground state calculations, we choose the following settings in ABINIT and Elk: Fermi-Dirac smearing of 0.001 Ha, and $8 \times 8 \times 8$ Monkhorst-Pack grid for Brillouin zone integration with (0.5, 0.5, 0.5) shift. In addition, we use planewave cutoff of $E_{\text{cut}} = 100$ Ha in ABINIT and the highest accuracy `vhighq` option in Elk. For the phonon calculations, we employ the density functional perturbation theory (DFPT) [39] feature in ABINIT. Note that since we have used a surrogate parameter for the planewave energy cutoff, we also determine the planewave energy cutoff in ABINIT corresponding to an accuracy in energy (with respect to discretization) of $\delta_E = 10^{-3}$ and 10^{-4} Ha/atom, as typical in practice, by choosing a simple cubic unit cell with equilibrium lattice constant determined by all-electron calculations,¹ Fermi-Dirac smearing of 0.001 Ha, and $8 \times 8 \times 8$ Monkhorst-Pack grid for Brillouin zone integration with (0.5, 0.5, 0.5) shift. Once all these metrics have been calculated, the pseudopotential with the desired accuracy and maximal softness is selected.

5. Results and discussion

We now use the aforescribed formulation and implementation to generate a comprehensive table of soft and transferable ONCV pseudopotentials. In particular, we consider scalar relativistic pseudopotentials with nonlinear core corrections in the Perdew–Burke–Ernzerhof (PBE) [31] exchange–correlation approximation. Within our framework, we use ONCVSP 4.0.1, Elk 6.8.04, and ABINIT 8.10.3 for the construction of pseudopotentials, pseudopotential DFT calculations, and all-electron DFT calculations, respectively. The starting guess for the SPEA2 evolutionary algorithm, used to solve the multi-objective optimization (Eq. 5a), is a random set of pseudopotentials that belong to the feasible set P (Eq. 15). The input parameters for the ONCVSP code, other than those being optimized, are identical to those used to generate the standard-accuracy pseudopotentials in the PseudoDojo database [19].

¹Or by known equilibrium distances in isolated cases where the cubic system does not yield representative distances.

While in most cases highly accurate and soft potentials are generated directly, in some cases manual adjustments were required to improve transferability and/or smoothness. This can happen, for example, when the optimization is too aggressive in a given angular momentum channel, leading to sharp variations in projectors and/or insufficient log-derivative agreement with all-electron results. In most such cases, however, since the $\delta_{\Delta E}$ criterion targeted in the optimization encompasses a variety of crystal structures, the required adjustments were relatively straightforward, e.g., increasing q_c^l in a given channel and/or r_{loc} of the local part. In the relatively few cases where adjustments were less straightforward, adjustment of individual projector r_c^l , local part r_{loc} , and/or projector target energies was required to ensure desired smoothness and log-derivative agreement throughout the target spectrum.

5.1. Example: magnesium

To clarify the construction process in practice, we consider Mg as a representative example. In Fig. 2, we present the evolution of the Pareto frontier during the multi-objective optimization (Eq. 5a). It is clear that around 50 iterations/generations are sufficient to obtain a converged Pareto frontier, suggesting rapid convergence of the chosen evolutionary algorithm. Indeed, the number of iterations/generations required for convergence is dependent on the starting guess. The advantage of the developed formulation/implementation is that the pseudopotentials from the Pareto frontier can be used in subsequent efforts to generate optimized pseudopotentials, significantly accelerating convergence of the multi-objective optimization in such instances.

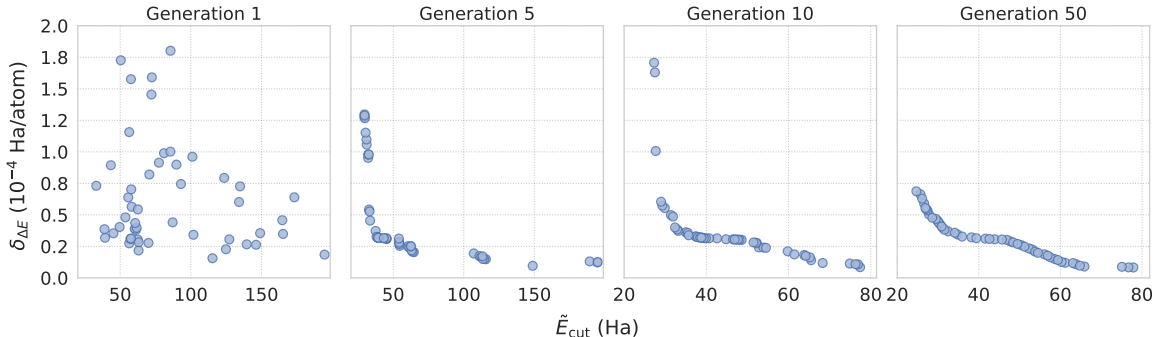


Figure 2: Evolution of the Pareto frontier during the multi-objective optimization for the Mg pseudopotential.

In Fig. 3, we plot the correlation between the error metric $\delta_{\Delta E}$ used in the multi-objective optimization (Eq. 5a) and the error metrics Δ , δ_{lat} , δ_{asr} , and δ_{ω} used for the selection (Eq. 5b) of the pseudopotential from the Pareto frontier so generated. It is clear from the results that the chosen error metrics are not significantly correlated, providing motivation for their use in this work. In particular, as discussed before, $\delta_{\Delta E}$ is not designed to be a *universal* metric for determining the accuracy of pseudopotentials, but rather a computationally feasible one that can provide a good estimate of accuracy and transferability. Indeed, since Δ , δ_{lat} , δ_{asr} , and δ_{ω} are not significantly correlated with $\delta_{\Delta E}$, choosing all of them as part of the optimization problem is expected to produce pseudopotentials that are generally more transferable. It is also worth noting that more transferable pseudopotentials, as estimated by the error metrics considered, are not necessarily harder. This provides a key motivation for a systematic, optimization based approach.

5.2. Table of ONCV pseudopotentials

We now use the developed framework to generate a table of soft and transferable pseudopotentials for the sixty-nine chemical elements H–La and Hf–Bi (<https://github.com/SPARC-X/SPMS-psps>).

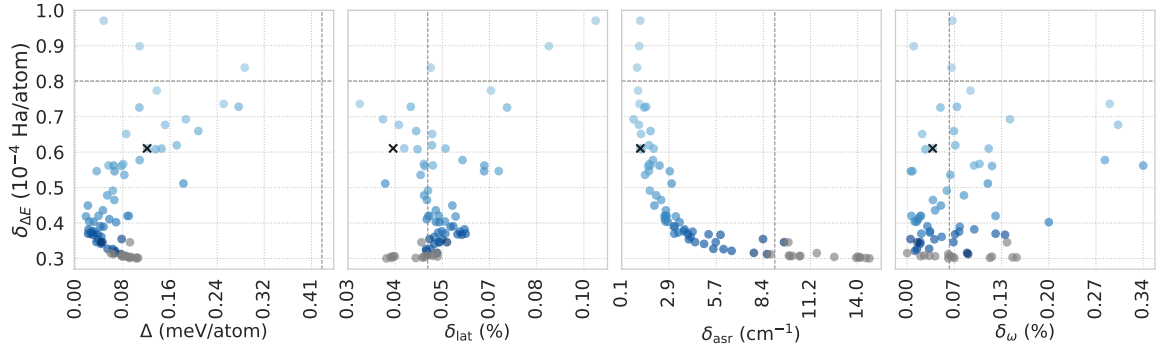


Figure 3: Correlation between the error metric $\delta_{\Delta E}$ used in the multi-objective optimization and the error metrics Δ , δ_{lat} , δ_{asr} , and δ_{ω} used for the selection of the pseudopotential from the Pareto frontier, for magnesium. The dashed lines indicate the results for the PseudoDojo standard-accuracy pseudopotential. The shading used for the markers represents the softness of the pseudopotential, with lighter shades corresponding to softer pseudopotentials. The gray color is used to represent pseudopotentials that are harder than PseudoDojo. The chosen pseudopotential is marked by the cross symbol.

The upper bounds of the error metrics, ϵ_1 , ϵ_2 , ϵ_3 , and ϵ_4 (Eq. 5b) are chosen such that the present table has an accuracy comparable to that of the standard-accuracy PseudoDojo table [19]. In Fig. 4, we present a summary of the softness and error metric values obtained for the present table, standard-accuracy PseudoDojo table [19], and SG15 table [18] for comparison. Detailed results and comparisons for each chemical element are available at the SPMS-psps website. It is clear from the results that the present pseudopotentials have comparable accuracy to the PseudoDojo pseudopotentials, while being significantly softer. In particular, the average E_{cut} to achieve $\delta_E = 10^{-3}$ Ha/atom is 18.7 Ha for the present table compared to 29.1 Ha for PseudoDojo. The corresponding numbers for $\delta_E = 10^{-4}$ Ha/atom are 22.6 Ha and 34.4 Ha, respectively. These results translate to $\sim 2\times$ speedups in diagonalization-based DFT calculations having energy errors in the range 10^{-3} to 10^{-4} Ha/atom as typical in practice. The speedups are significantly larger in the case of linear-scaling methods, particularly those that do not employ a reduced basis, e.g., speedups of $\sim 5\times$ are expected for the spectral quadrature method [40, 41]. It is also clear from the results that the present table of pseudopotentials is softer than the SG15 table while more accurate based on the metrics considered. Indeed, it is possible to choose ϵ_1 , ϵ_2 , ϵ_3 , and ϵ_4 such that the present table of pseudopotentials has comparable accuracy to SG15, in which case the pseudopotentials generated could be made even softer.

6. Concluding remarks

In this work, we employed multi-objective optimization to maximize pseudopotential softness while maintaining high accuracy and transferability. We developed a formulation (Eqs. 5a and 5b) in which softness and accuracy are simultaneously maximized, with accuracy $\delta_{\Delta E}$ (Eq. 3a) determined by the ability to reproduce all-electron energy differences between Bravais lattice structures, after which the resulting Pareto frontier is scanned for the softest pseudopotential that provides the desired accuracy in established transferability tests: Δ -factor, lattice constant of GBRV structures, violation of acoustic sum rule in phonon calculations, and convergence of phonon frequencies. We employed an evolutionary algorithm to solve the multi-objective optimization problem and applied it to generate a table of ONCV pseudopotentials (<https://github.com/SPARC-X/SPMS-psps>) for the sixty-nine chemical elements H–La and Hf–Bi within the PBE exchange-correlation approximation. We find that the resulting table is softer than the current PseudoDojo table of comparable accuracy and more accurate than the current SG15 table of comparable softness, according to the standard metrics considered.

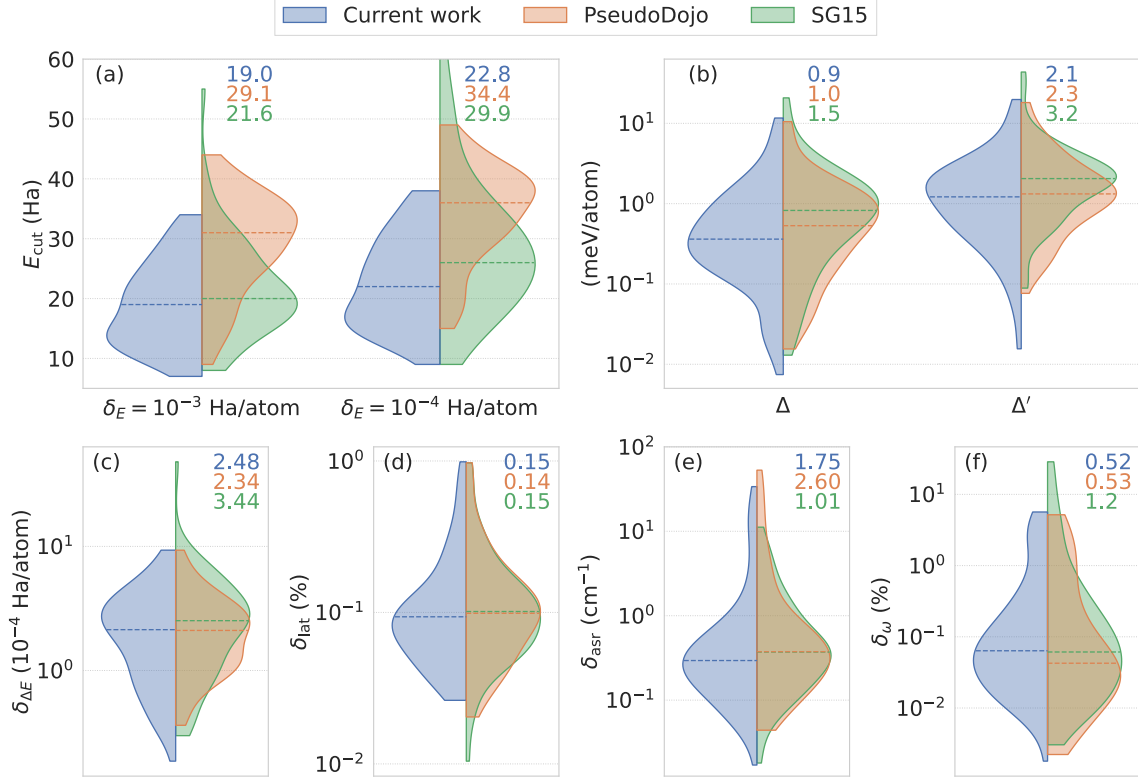


Figure 4: Overview of the softness and error metric values obtained for the present, SG15 [18], and standard-accuracy PseudoDojo [19] tables of pseudopotentials. The horizontal dashed lines correspond to median values and the numbers listed correspond to the mean values.

Overall, the pseudopotentials generated using the proposed formulation/implementation are expected to significantly accelerate Kohn-Sham DFT calculations while maintaining accuracy comparable to existing high quality tables. Indeed, initial versions of the pseudopotentials have already been successfully applied in the study of a number of low-dimensional systems [42, 43, 44]. The development of error metrics that provide a better quantification of accuracy and transferability, while remaining computationally tractable, is likely to further improve the quality and/or softness of the generated pseudopotentials, making it a worthy subject for future research. The generation of tables including spin-orbit coupling and additional exchange-correlation approximations will also be of interest to pursue.

Acknowledgments

This work was supported by grant DE-SC0019410 funded by the U.S. Department of Energy, Office of Science. This work was performed in part under the auspices of the U.S. Department of Energy by Lawrence Livermore National Laboratory under Contract DE-AC52-07NA27344. J.E.P gratefully acknowledges D. R. Hamann for invaluable discussions regarding the construction of ONCV pseudopotentials over the years. The views and conclusions contained in this document are those of the authors and should not be

interpreted as representing the official policies, either expressed or implied, of the Department of Energy, or the U.S. Government.

References

- [1] P. Hohenberg and W. Kohn. Inhomogeneous electron gas. *Phys. Rev.*, 136:B864–B871, 1964.
- [2] W. Kohn and L. J. Sham. Self-consistent equations including exchange and correlation effects. *Physical Review*, 140(4A):A1133, 1965.
- [3] R. Martin. *Electronic Structure: Basic theory and practical methods*. Cambridge University Press, 2004.
- [4] D. Vanderbilt. Soft self-consistent pseudopotentials in a generalized eigenvalue formalism. *Phys. Rev. B*, 41:7892–7895, 1990.
- [5] P. E. Blöchl. Projector augmented-wave method. *Phys. Rev. B*, 50:17953–17979, 1994.
- [6] D. R. Hamann, M. Schlüter, and C. Chiang. Norm-conserving pseudopotentials. *Phys. Rev. Lett.*, 43:1494–1497, 1979.
- [7] G. P. Kerker. Non-singular atomic pseudopotentials for solid state applications. *J. Phys. C: Solid State Phys.*, 13(9):L189, 1980.
- [8] G. B. Bachelet, D. R. Hamann, and M. Schlüter. Pseudopotentials that work: From H to Pu. *Phys. Rev. B*, 26:4199–4228, 1982.
- [9] D. R. Hamann. Generalized norm-conserving pseudopotentials. *Phys. Rev. B*, 40:2980–2987, 1989.
- [10] A. M. Rappe, K. M. Rabe, E. Kaxiras, and J. D. Joannopoulos. Optimized pseudopotentials. *Phys. Rev. B*, 41:1227–1230, 1990.
- [11] N. Troullier and J. L. Martins. Efficient pseudopotentials for plane-wave calculations. *Phys. Rev. B*, 43:1993–2006, 1991.
- [12] S. Goedecker, M. Teter, and J. Hutter. Separable dual-space Gaussian pseudopotentials. *Phys. Rev. B*, 54:1703–1710, 1996.
- [13] C. Hartwigsen, S. Goedecker, and J. Hutter. Relativistic separable dual-space Gaussian pseudopotentials from H to Rn. *Phys. Rev. B*, 58:3641–3662, 1998.
- [14] D. R. Hamann. Optimized norm-conserving Vanderbilt pseudopotentials. *Phys. Rev. B*, 88(8):085117, 2013.
- [15] T. L. Beck. Real-space mesh techniques in density-functional theory. *Rev. Mod. Phys.*, 72(4):1041–1080, 2000.
- [16] S. Yousef, J. R. Chelikowsky, and S. M. Shontz. Numerical methods for electronic structure calculations of materials. *SIAM Review*, 52(1):3–54, 2010.
- [17] Q. Xu, A. Sharma, B. Comer, H. Huang, E. Chow, A. J. Medford, J. E. Pask, and P. Suryanarayana. SPARC: Simulation package for ab-initio real-space calculations. *SoftwareX*, 15:100709, 2021.

- [18] M. Schlipf and F. Gygi. Optimization algorithm for the generation of ONCV pseudopotentials. *Comput. Phys. Commun.*, 196:36–44, 2015.
- [19] M. J. Van Setten, M. Giantomassi, E. Bousquet, M. J. Verstraete, D. R. Hamann, X. Gonze, and G-M Rignanese. The PseudoDojo: Training and grading a 85 element optimized norm-conserving pseudopotential table. *Comput. Phys. Commun.*, 226:39–54, 2018.
- [20] K. F. Garrity, J. W. Bennett, Karin M. Rabe, and D. Vanderbilt. Pseudopotentials for high-throughput DFT calculations. *Comput. Mater. Sci.*, 81:446–452, 2014.
- [21] G. Kresse and D. Joubert. From ultrasoft pseudopotentials to the projector augmented-wave method. *Phys. Rev. B*, 59(3):1758, 1999.
- [22] F. Jollet, M. Torrent, and N. Holzwarth. Generation of projector augmented-wave atomic data: A 71 element validated table in the xml format. *Comput. Phys. Commun.*, 185(4):1246–1254, 2014.
- [23] M. Topsakal and R. M. Wentzcovitch. Accurate projected augmented wave (PAW) datasets for rare-earth elements (RE=La–Lu). *Comput. Mater. Sci.*, 95:263–270, 2014.
- [24] M. Krack. Pseudopotentials for H to Kr optimized for gradient-corrected exchange-correlation functionals. *Theor. Chem. Acc.*, 114(1):145–152, 2005.
- [25] PARSEC TM pseudopotentials: <https://parsec.oden.utexas.edu/styled-2>, accessed 2021-12-24.
- [26] M. Fuchs and M. Scheffler. Ab initio pseudopotentials for electronic structure calculations of polyatomic systems using density-functional theory. *Comput. Phys. Commun.*, 119(1):67–98, 1999.
- [27] A. Willand, Y. O. Kvashnin, L. Genovese, Á. Vázquez-Mayagoitia, A. K. Deb, A. Sadeghi, T. Deutsch, and S. Goedecker. Norm-conserving pseudopotentials with chemical accuracy compared to all-electron calculations. *J. Chem. Phys.*, 138(10):104109, 2013.
- [28] A. Dal Corso. Pseudopotentials periodic table: From H to Pu. *Comput. Mater. Sci.*, 95:337–350, 2014.
- [29] E. Kucukbenli, M. Monni, B. I. Adetunji, X. Ge, G. A. Adebayo, N. Marzari, S. de Gironcoli, and A. Dal Corso. Projector augmented-wave and all-electron calculations across the periodic table: a comparison of structural and energetic properties. *arXiv preprint arXiv:1404.3015*, 2014.
- [30] G. Prandini, A. Marrazzo, I. E. Castelli, N. Mounet, and N. Marzari. Precision and efficiency in solid-state pseudopotential calculations. *Npj Comput. Mater.*, 4(1):1–13, 2018.
- [31] J. P. Perdew, K. Burke, and M. Ernzerhof. Generalized gradient approximation made simple. *Phys. Rev. Lett.*, 77(18):3865, 1996.
- [32] K. Lejaeghere, V. Van Speybroeck, G. Van Oost, and S. Cottenier. Error estimates for solid-state density-functional theory predictions: an overview by means of the ground-state elemental crystals. *Crit. Rev. Solid State Mater. Sci.*, 39(1):1–24, 2014.
- [33] K. Lejaeghere, G. Bihlmayer, T. Björkman, P. Blaha, S. Blügel, V. Blum, D. Caliste, I. E. Castelli, S. J. Clark, A. Dal Corso, et al. Reproducibility in density functional theory calculations of solids. *Science*, 351(6280), 2016.

- [34] D. R. Hamann. Erratum: Optimized norm-conserving Vanderbilt pseudopotentials [Phys. Rev. B 88, 085117 (2013)]. *Phys. Rev. B*, 95:239906, 2017.
- [35] ONCVSP code: <http://www.mat-simresearch.com>, accessed 2021-12-24.
- [36] X. Gonze, J. M. Beuken, R. Caracas, F. Detraux, M. Fuchs, G. M. Rignanese, L. Sindic, M. Verstraete, G. Zerah, F. Jollet, M. Torrent, A. Roy, M. Mikami, P. Ghosez, J. Y. Raty, and D. C. Allan. First-principles computation of material properties: the ABINIT software project. *Comp. Mater. Sci.*, 25:478–492(15), 2002.
- [37] The Elk code: <http://elk.sourceforge.net>, accessed 2021-12-24.
- [38] E. Zitzler, M. Laumanns, and L. Thiele. SPEA2: Improving the strength pareto evolutionary algorithm. *TIK-report*, 103, 2001.
- [39] X. Gonze. Adiabatic density-functional perturbation theory. *Phys. Rev. A*, 52(2):1096, 1995.
- [40] P. Suryanarayana, P. P. Pratapa, A. Sharma, and J.E. Pask. SQDFT: Spectral Quadrature method for large-scale parallel O(N) Kohn–Sham calculations at high temperature. *Computer Physics Communications*, 224:288–298, 2018.
- [41] P. Suryanarayana. On spectral quadrature for linear-scaling density functional theory. *Chemical Physics Letters*, 584:182–187, 2013.
- [42] A. Bhardwaj and P. Suryanarayana. Elastic properties of Janus transition metal dichalcogenide nanotubes from first principles. *The European Physical Journal B*, 95(1):1–8, 2022.
- [43] A. Bhardwaj and P. Suryanarayana. Strain engineering of Janus transition metal dichalcogenide nanotubes: an ab initio study. *The European Physical Journal B*, 95(3):1–9, 2022.
- [44] S. Kumar and P. Suryanarayana. On the bending of rectangular atomic monolayers along different directions: an ab initio study. *arXiv preprint arXiv:2208.00091*, 2022.